Nuclear magnetic resonance spin-lattice relaxation of lithium ions in aqueous solution by NMR and molecular dynamics

Mohaddese Mohammadi[a], Stefan Benders[a], Alexej Jerschow*[a]

[a] Department of Chemistry, New York University, 100 Washington Square East, New York, New York, 10003, USA.

AUTHOR INFORMATION

Corresponding Author

*alexej.jerschow@nyu.edu

ABSTRACT

We study the aqueous solvation dynamics of lithium ions using NMR spectroscopy, molecular dynamics, and viscosity measurements. Several relaxation mechanisms are examined to explain the strong increases of spin-lattice relaxation towards high concentrations. The use of both ^{6}Li and ^{7}Li isotopes is helpful to separate out the quadrupolar contribution to the relaxation rate. In particular, it is found that the quadrupolar interaction constitutes the strongest contribution above a concentration of approximately 10 molal. The next-strongest contribution arises from interactions that scale with the square of the gyromagnetic ratio (mostly the dipolar interaction), and the experimental relaxation rates appear to be fully accounted for when these mechanisms are combined over the concentration range up to the saturation concentration. The study of solvation dynamics, particularly at high concentrations could be of relevance for electrolyte dynamics in aqueous Li-ion rechargeable batteries.

1. INTRODUCTION

Lithium solutions are of particular interest due to their use in rechargeable batteries[1]. While typically an organic solvent is used as a matrix for lithium salts, the use of an aqueous environment has been examined recently[2]. Aqueous solutions are significantly safer[3–5], but their stable electrochemical window is only about 1.23 V, which is too narrow to operate high capacity Li-ion battery devices[3]. The use of higher concentrations in aqueous solution can significantly broaden the stability window, thus enabling higher capacity devices on this basis. The understanding of the dynamics of solvation, especially at high concentrations, hence could provide insights into the charge transfer pathways[6]. Herein, we examine the behavior of lithium ions in aqueous solution through NMR relaxation and viscosity measurements, and compare the results with molecular dynamics simulations. The study is performed over a large concentration range up to the solubility limit (~20 molal).

There have been many efforts to determine the structure of the solvation shells of Li^+ ions using neutron diffraction, X-ray diffraction and infrared spectroscopy[7–9]. The fact that lithium has two NMR-active isotopes, ^{7}Li and ^{6}Li, provides opportunities for studying different NMR relaxation mechanisms and link them to dynamic and structural properties using NMR spectroscopy. Furthermore, the generally small quadrupolar moments of both isotopes (with ^{6}Li having a particularly small one), makes it possible to detect other, weaker relaxation mechanisms in certain situations. Figure 1 illustrates the relevant mechanisms that may be encountered in this situation.

Previous studies indicated that the ^{7}Li spin-lattice relaxation rate of LiCl in H_2O solutions was twice that of D_2O solutions in the range of 0-7 molal.[10,11]. This difference was explained by the ^{7}Li-^{1}H dipole-dipole interaction, with the rest being caused likely by the quadrupolar interaction. Other studies have further underlined the major contribution of the quadrupolar mechanism in ^{6}LiCl in H_2O and D_2O at 3.9 M concentration[12] and through proton relaxation measurements in ^{7}LiCl-H_2O and ^{6}LiCl-H_2O for up to 3 molal concentration.[13]

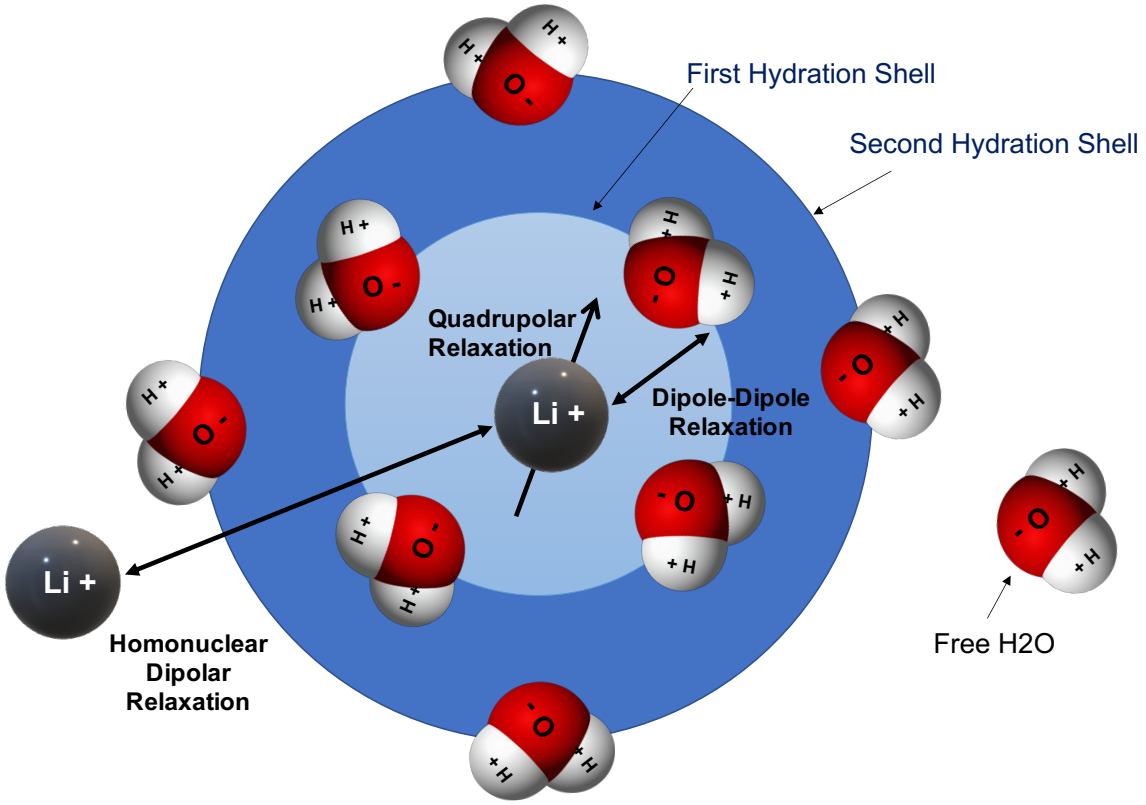

FIG. 1. Illustration of relaxations mechanism contributing in the overall relation rate of ^{7}Li ion in H_2O solvent.

Hertz et al[14] reported T_1 relaxation rates for ^{7}Li in H_2O and D_2O solutions of LiCl, LiBr, and LiI at concentrations ranging from 0 to 18 mol/L. Using these data, the authors calculated the rotational correlation time for the first hydration shell of Li^+ hydration shell and suggested a cubic symmetry in the hydration sphere at lower concentration. The quadrupolar and dipolar contributions were separated, and the changes in the quadrupolar contribution were interpreted as a change in the hydration symmetry at higher concentration. Both classical, and *ab initio* molecular dynamics were performed to study

solvation structure and dynamics of several alkali and earth alkali ions,[15–17] and revealed, among other things, curious collective water dynamics at low ion concentrations.

Here we examine the full concentration range between 0 and 20 molal and study the T_1 relaxation of ^{6}Li and ^{7}Li solutions in H_2O and D_2O in order to examine and separate out the different relaxation mechanisms over the whole concentration range. Viscosity and diffusion measurements provide additional parameters towards this analysis. In addition, molecular dynamics (MD) simulations, show that the major relaxation contributions must arise from the quadrupolar interaction, and a combination between these calculated values and experimental data from both isotopes produces an excellent account for the total ^{7}Li relaxation rate over the whole concentration range.

2. EXPERIMENTAL SECTION

2.1. Sample Preparation.

All NMR samples were prepared in 5 mm NMR tubes. In order to keep the sample preparation simple and consistent, the volume of solvent was kept constant and the concentration and molality of the sample were determined by the mass of salt added to the solvent. H_2O-based solvent was prepared with 90% deionized H_2O and 10% D_2O and D_2O-based solvent was 99.99% D_2O. ^{6}LiCl salt was composed of 99.95% - enriched ^{6}Li isotope. The masses of ^{6}LiCl and ^{7}LiCl salts were measured with a laboratory scale to 0.1 mg accuracy. The accuracies of solutions' concentrations were verified using their NMR signal ratios.

The kinematic viscosity of liquids was measured using a Cannon-Ubbelohde calibrated semi-micro viscometer with the kinematic viscosity range of 1600-8000 mm^2/s. To calculate the dynamic viscosity of solutions, the relationship between the viscosities of solvent and solution and their densities, $\eta_r = \frac{\eta}{\eta_0} = \frac{t\rho}{t_0\rho_0}$, where t and t_0 are the efflux times for the solution and solvent, was used. Densities were determined by measuring the weight

of 1mL of the solutions. The temperature was kept constant at 22ºC during the viscosity measurements.

2.2. Nuclear Magnetic Resonance spectroscopy**.**

All NMR experiments were performed on a Bruker 9.4 T Avance I spectrometer with a Bruker Micro2.5 gradient assembly and on a Bruker 11 T Avance I spectrometer for high resolution spectroscopy. T_1 relaxation of solutions at different concentrations was measured using the inversion recovery pulse sequence. The recycle delay was set to 1000 s for ^{6}Li samples and to 15-200 s for ^{7}Li solutions, depending on the concentration, with two scans to perform a 0º, 180º phase cycle on the 180º pulse. The 90º and 180º pulse durations used in ^{7}Li inversion-recovery experiments were 40 μs and 81 μs for the 9.4T instrument and 12 μs and 24 μs for the 11T instrument. For ^{6}Li the pulse durations were 80 μs and 161 μs for the 90º and 180º pulses on the 9.4 T instrument. To increase the accuracy of reported data, the measurements were repeated three times with different samples as indicated in the results section. Lithium self-diffusion was measured in order to examine any unusual lengthening of translational correlation times at larger concentrations using the bipolar pulsed field gradient sequence of Figure S2. The results are shown in Figure S6 and S7. To implement the experiment, we used the DOSY topspin macro with the gradient power ranging from 2 % to 95 %. The temperature was calibrated using ethylene glycol. The gradient power was calibrated using proton diffusion measurements at 22 ºC. The spectral window for all measurements was approximately 80 ppm.

2.3. Molecular Dynamics Simulation

Molecular dynamics simulations were performed using the OpenMM package v. 7.1 on NYU's high-performance computing platform with the following methods and parameters: The system was created with the requisite molality of LiCl in SPCE water in a 40×40×40 nm^3 box with periodic boundary conditions. Calculations were performed with nonbonded cutoff of 1 nm, nonbonded method – PME, a time step 2 fs, a temperature of 295.15 K (to match experiments), a pressure of 1 atm (Monte Carlo barostat with an interval of 25 steps), 100,000 equilibration steps, 200,000 production steps (400 ps), and a

Langevin integrator. Following energy minimization and NPT equilibration, production runs were performed. The analysis was performed using the Python mdanalysis package in order to obtain the relevant correlation functions as described below. Correlation functions were fit to a biexponential decay.

3. RESULTS AND DISCUSSION

Figure 2 shows the comparison between the ^{7}Li T_1 relaxation rates of H_2O (curve 1) and D_2O solutions (curve 2). As is seen clearly, over the whole concentration range, the rates are lower for the D_2O samples. There are two reasons for such a difference: (1) the viscosity of D_2O is larger than the viscosity of H_2O, and (2) there is an additional contribution from the dipolar relaxation mechanism in the H_2O sample due to ^{7}Li-^{1}H couplings. Figure 3 shows the viscosity measurements of both sets of solutions. Since in the fast motion regime, which applies here, the correlation time is proportional to viscosity, one can correct for the viscosity effect by scaling the relaxation rate as $R_{1,\mathrm{sol1}} = R_{1,\mathrm{sol2}} \frac{\eta_{\mathrm{sol1}}}{\eta_{\mathrm{sol2}}}$, where $R_{1,\mathrm{sol}i}$ and $\eta_{\mathrm{sol}i}$ are the spin-lattice relaxation rate and viscosity of the i-th solution, respectively. Density measurements are used to convert from kinematic viscosity to dynamic viscosity. With this adjustment, curve 3 in Fig. 2 shows the ^{7}Li relaxation rate in H_2O without the contribution from the ^{1}H-^{7}Li relaxation. This curve is the basis for exploring which other relaxation mechanisms need to be considered. It is clear that the dipolar contribution shows a relatively minor effect over most of the concentration range, with the biggest fraction occurring at the lower concentrations.

At this stage, it is also useful to explore whether ^{7}Li-^{7}Li dipolar interactions or even ^{7}Li-^{35,37}Cl interactions could lead to additional relaxation contributions. Given the radial distribution functions (Fig. 4) obtained from molecular dynamics simulations, it appears that protons are the closest NMR-active nuclei to the ^{7}Li nuclei in solution. Therefore other relaxation contributions would be weaker than the ^{7}Li-^{1}H portion as given by the relative factor $\frac{\gamma_m^2 I_m(I_m+1)/r_m{}^3}{\gamma_n^2 I_n(I_n+1)/r_n^3}$, where $\gamma_{m,n}$ and $I_{m,n}$ are the gyromagnetic ratios and the spin values for the two isotope types that are compared and $r_{m,n}$ is their average distance to ^{7}Li nuclei.

This analysis shows that the ^{7}Li-^{35}Cl contribution would be scaled by 0.048 and the one for ^{7}Li-^{37}Cl by 0.033 when compared to ^{7}Li-^{1}H (assuming same distances). Similarly, the ^{7}Li-^{2}D contribution would be relatively small, scaled by 0.0628 compared to ^{7}Li-^{1}H. The ^{7}Li-^{7}Li contribution would be relatively comparable to ^{7}Li-^{1}H (scaling factor 0.755). The average distances, however, are much larger for ^{7}Li-^{7}Li (the first radial distribution function peak appears at 5.5Å for ^{7}Li-^{7}Li, and 2.6Å for ^{7}Li-^{1}H) as evidenced in the calculated radial distribution functions in Fig. 4. Furthermore, the concentration of ^{7}Li is always significantly lower than the ^{1}H concentration. At very high concentrations, there is another radial distribution function peak at 4.0Å. The conclusion here is therefore that the most significant interaction comes from the ^{7}Li-^{1}H dipolar couplings, which causes the difference seen between curves 1 and 3.

The potential contribution of paramagnetic oxygen to relaxation was considered as follows: samples of ^{6}Li at 0.5 mol/L were measured in H_2O and D_2O with and without degassing by three freeze-pump-thaw cycles and flame-sealing. For the D_2O sample, the T_1 was found to be 525 s before, and 780 s after degassing. For the H_2O sample, the T_1 was found to be 168 s before, and 189 s after degassing. These results indicate that the contribution to the relaxation rate from oxygen-induced relaxation is approximately R_1^{ox} =6.22*10^{-4} s^{-1} in the first case and 6.61*10^{-4} s^{-1} in the second case. Both values lie within the experimental error of the procedure and suggest that the relaxation contribution is outside of the detectable range, given the strength of the other mechanisms. Taking the larger of the two, and predicting the value for ^{7}Li, by considering the square of the relative gyromagnetic ratios $\frac{\gamma_{7Li}^2}{\gamma_{6Li}^2}$, , one obtains 0.0046 s^{-1}, which is also significantly smaller than the observed rates for ^{7}Li. Therefore, we conclude that the influence of oxygen can be neglected in the relaxation analysis under the current conditions.

The comparison between ^{7}Li and ^{6}Li relaxation, curves 1 and 4, can answer the question of whether and how much quadrupolar relaxation contributes to the observed rates. The quadrupolar relaxation rate is given by[18]

$$R_{1Q} = \frac{3}{100}\left(\frac{eQ(2I+3)}{I(2I-1)\hbar}\right)^2 \left(J_V(\omega) + 4J_V(2\omega)\right), \quad (1)$$

where e is the electronic charge, Q is the nuclear quadrupole moment, I is the nuclear spin value, $\hbar$ Planck's constant divided by 2π, and $J_V(\omega)$ the spectral density function for the electric field gradient at the angular frequency ω. We note that differences in numerical prefactors are often found in the literature but typically can be traced to differences in the definitions of the spectral density functions and electrical field gradients[18]. We describe the definition used here explicitly below.

The nuclear quadrupole moments Q for the ^{7}Li and ^{6}Li used were -4.01 fm^2 and -0.0808 fm^2, respectively[19,20]. Using the relative spin values (3/2 for ^{7}Li and 1 for ^{6}Li), one can obtain the scaling factor 3546.7 for the difference between the ^{7}Li quadrupolar relaxation contribution and the one for ^{6}Li. The ratio between the experimental ^{7}Li and ^{6}Li relaxation rates, however, ranges only from 10-50 over the whole concentration range (Fig S4). Therefore, one can conclude that the majority of the ^{6}Li relaxation rate is not caused by quadrupolar relaxation. Other interactions, such as the dipolar interaction and the chemical shift interaction scale as the square of the ratio of the gyromagnetic ratio between the two isotopes. When applying this scaling to curve 4, one obtains a contribution that is similar in size as the difference between curves 1 and 3 over the whole concentration range, especially at higher concentrations.

Following this analysis, the hypothesis now stands that the majority of the ^{7}Li relaxation mechanism has to be caused by the quadrupolar mechanism at concentrations above approximately 7 molal. This interaction is almost nonexistent (by comparison) for ^{6}Li. This proposition was tested using molecular dynamics (MD) simulations. Previously, MD at varying levels of theory was used to extract quadrupolar relaxation rates for ions in aqueous solutions at low concentrations[17,21]. Here we performed classical molecular dynamics simulations and with a point-charge approximation to calculate the electric field gradient (EFG) around the lithium ions at each time step, from which the requisite spectral density functions were calculated.

The spectral density is given by

$$J_V(\omega) = FT\{C_V(t)\} = FT\{\langle V_{zz}(t)V_{zz}(0)\rangle\}, \quad (2)$$

where FT denotes the Fourier transform, and $C_V(t)$ the correlation function. The EFG tensor V_{ij} is approximated using the point-charge approximation[22,23] for each MD snapshot using

$$V_{ij} = (1 + \gamma_\infty) \sum_k q_k \left(\frac{3 r_i r_j}{r^5} - \frac{\delta_{ij}}{r^3}\right), \quad (3)$$

where r_i are the components of the interatomic vector $\mathbf{r}$ between the central lithium ion and all other atoms, δ_{ij} is the Kronecker delta, q_k are the effective atomic charges, and γ_∞ is the Sternheimer antishielding factor accounting for the core electron polarization of the lithium ion, here taken to be 0.17. The charges were obtained from the force field as -0.8476e for oxygen, 0.4238e for hydrogen, and +e and -e for Li^+ and Cl^-, respectively. The EFG needed for calculating the quadrupolar relaxation contribution is a non-local quantity, which requires the use of very large clusters for calculations. The problem is exacerbated when MD is involved, since the calculation would have to be performed for each snapshot. Advanced methods based on polarized force field and ab initio molecular dynamics calculations have been demonstrated[15,21], but there does not yet exist a consensus as to which approach will converge to become the most reliable one while maintaining computational efficiency. By contrast, the point charge approximation is very powerful, due to its simplicity, can be computed efficiently for very large clusters and large trajectories, and provides good agreement with experimental results as shown below.

The averaging over the autocorrelation function for the electric field gradient in Eq. (2) is performed via the following relationship (using the convolution theorem),

$$C_V(t) = \langle V_{zz}(t) V_{zz}(0) \rangle = \frac{2}{3} iFT \left\{ \frac{1}{N_p} \sum_{i,j,p} V_{ij}^{(p)*}(\omega)\, V_{ij}^{(p)}(\omega) \right\}, \quad (4)$$

where $V_{ij}^{(p)}(\omega)$ are the Fourier transforms of the components of the electric field gradient tensor for the p-th lithium ion, N_p is the number of lithium ions in the box, iFT denotes the inverse Fourier transform, and the asterisk indicates complex conjugation. The factor $\frac{2}{3}$ arises from the difference between the Frobenius norm (calculated here), and the principal tensor component required in Eq. (2). The correlation functions of Eq. (4) were fit by a biexponential decay giving the intensities and time constants for the two components as a

and τ_a, and b and τ_b, respectively. With these values, the spectral densities were determined by

$$J_V(\omega) = \langle (V_{zz}(0))^2 \rangle \left(a \frac{\tau_a}{1+(\omega\tau_a)^2} + b \frac{\tau_b}{1+(\omega\tau_b)^2} \right). \quad (5)$$

The final result is shown in Figure 2, curve 6, which confirms that the major contribution to relaxation accounts for the quadrupolar interaction over most of the concentration range (at higher concentrations the behavior is better appreciated when looking at the linearly-scaled graph, as shown in Fig. S1). We can now use the ^{6}Li relaxation data as a source of information about the level of the non-quadrupolar contributions. These should be scaled by $(\gamma_{7Li}/\gamma_{6Li})^2$ if they are primarily due to dipolar coupling or chemical shift anisotropy. Adding this scaled contribution to the quadrupolar component from the MD calculation produces curve 5. This curve reproduces the overall experimental result very nicely over the whole concentration range within acceptable error. In addition, a comparison between the ^{7}Li relaxation data at 400 and 500 MHz showed very small differences (Fig. S5). Therefore one may deduce that the chemical shift anisotropy contributes a negligible relaxation effect over the whole concentration range.

To exclude other possible sources of the observed rise in ^{6}Li relaxation at higher concentrations, radiation damping (RD) was considered as a mechanism for the ^{6}Li experiments and was checked by performing the following experiments: Since RD strongly depends on the filling factor, we reduced the amount of liquid and performed the inversion recovery experiment again. The result was well inside the error range. To perform an additional test, we de-shimmed the signal to get a broader signal, then performed the inversion recovery and still got the same results. The intensity profile as a function of flip angle showed a standard nutation curve as well, which is a good indicator for the absence of RD[24]. Moreover, the characteristic line-shape of the radiation-damped signal[25] was never observed in ^{6}LiCl nor ^{7}LiCl high concentration samples. Therefore, one may conclude that RD is unlikely to be the reason for the increases in measured relaxation rates at high concentrations. The spin-rotation relaxation mechanism has previously been determined to be too weak to be observed under the current conditions, and we have not seen any indication to the contrary[26].

The significant increase of the quadrupolar relaxation contributions, especially beyond concentrations of 10 molal are particularly interesting, and likely arise from the reduced ability of water to symmetrize the lithium atoms and from more prolonged correlation times at high concentrations. The desymmetrization aspect for the lithium ions has also been mentioned by other authors[11]. To support this hypothesis, we examined the coordination numbers for the MD trajectories. Figure 4 shows a steady decrease of coordinating water in both the first and second coordination shells. In the first shell, the average number of waters decreases from ~4.3 to 2.3 as the concentration is increased, which indicates significant lack of symmetrization propensity for the ion. As expected, the Cl^- coordination increases with increasing concentrations in both coordination shells. Both second coordination shells flatten towards higher concentrations, as a consequence of crowding.

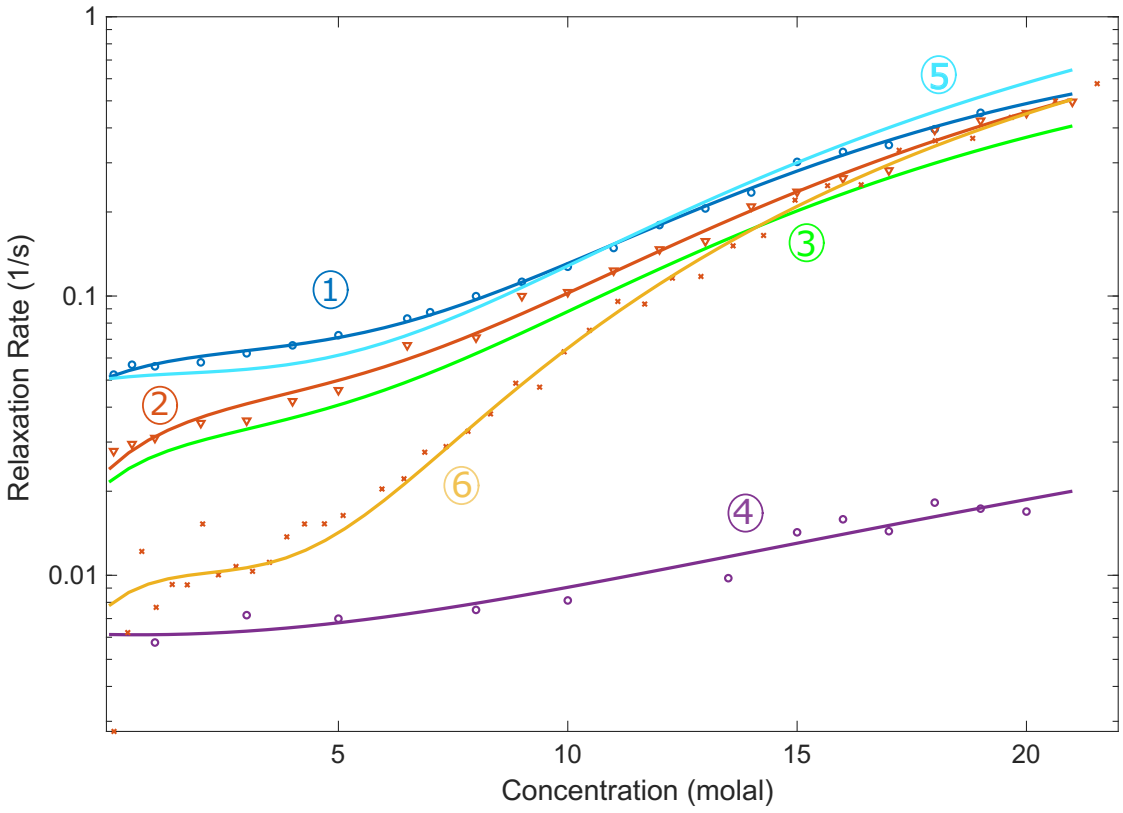

FIG. 2. Relaxation rate ($\frac{1}{T_1}$) of ^{7}Li and ^{6}Li in D_2O and H_2O in the concentration range of 1-20 molal (mol/kg). Curve 1: ^{7}LiCl-H_2O, Curve 2: ^{7}LiCl-D_2O, Curve 3: ^{7}LiCl-D_2O adjusted for relative viscosity to compare with Curve 1, Curve 4: ^{6}LiCl-H_2O, Curve 5: ^{7}Li quadrupolar relaxation contribution plus scaled ^{6}LiCl relaxation contribution (matches Curve 1), Curve 6: ^{7}Li quadrupolar relaxation contribution calculated from MD simulation. Solid lines represent polynomial fits through the experimental and computational data points.

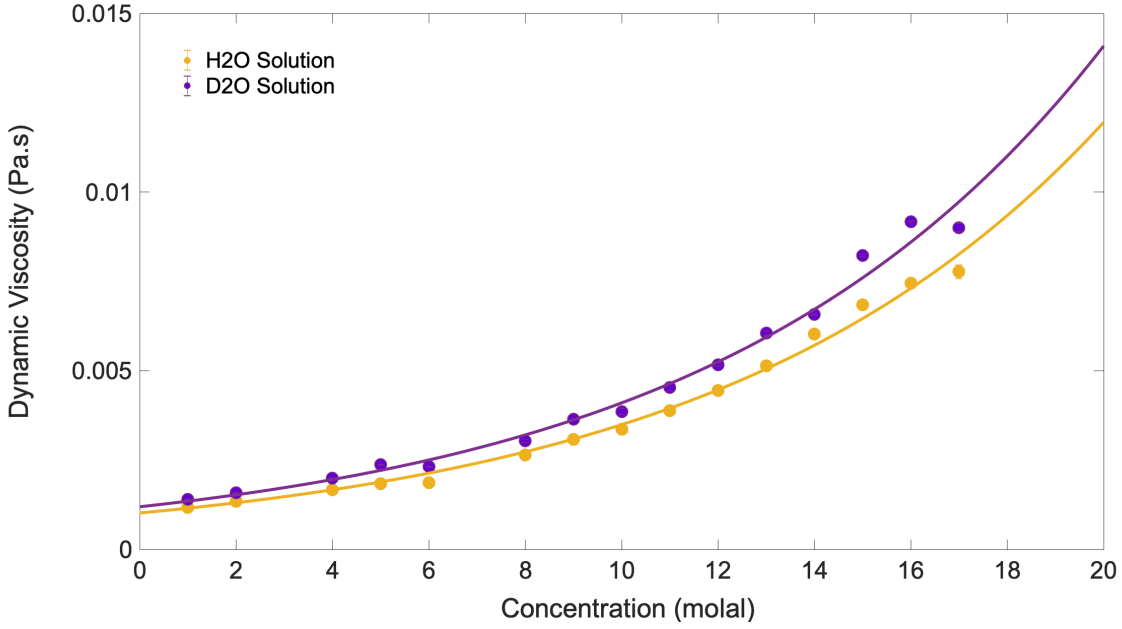

FIG. 3. Dynamic viscosity measurements of H_2O/D_2O solutions

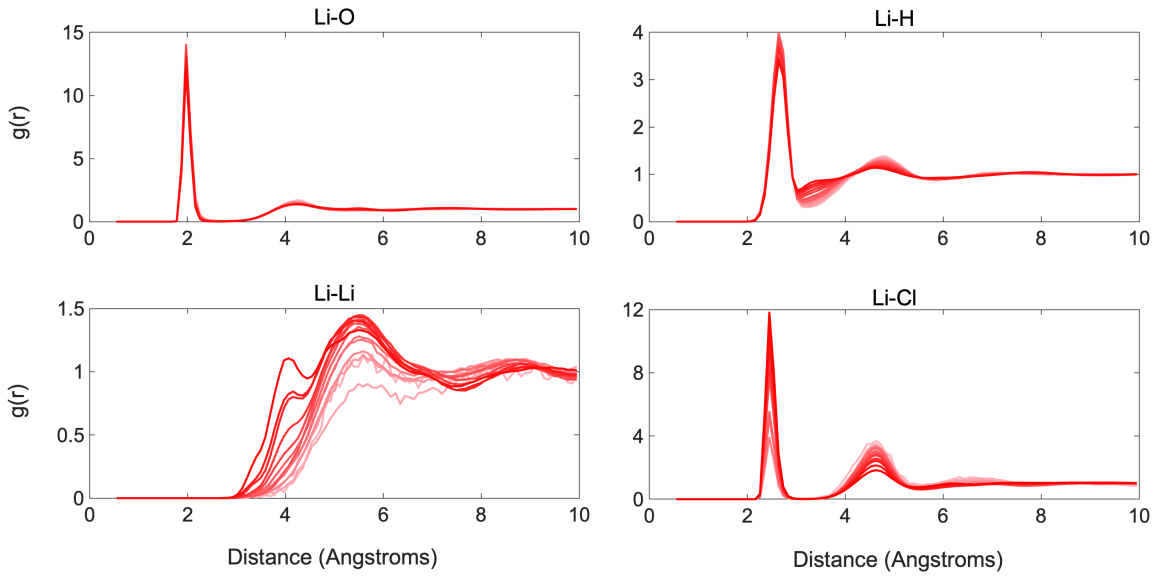

FIG. 4. Radial distribution functions for the indicated ion or atom pairs for the different ion concentrations. Curves are plotted from low (faded color) to high concentrations (full color).

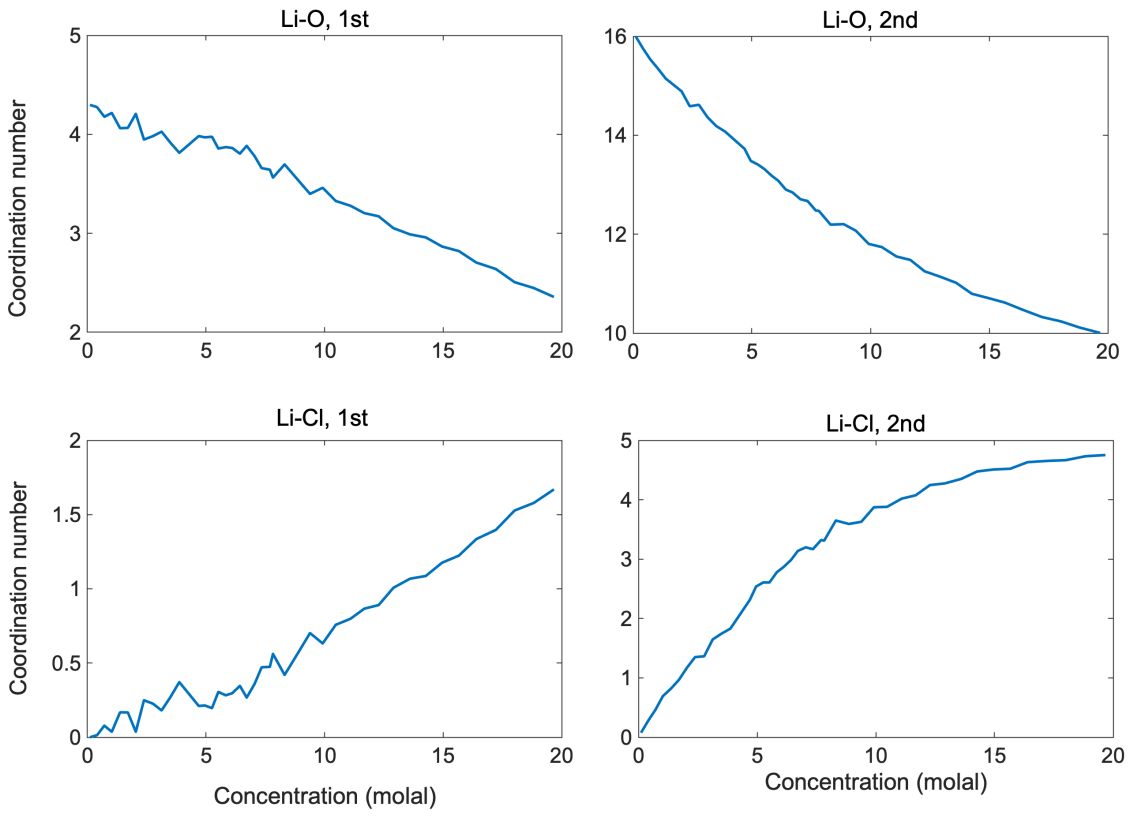

FIG. 5. Coordination numbers in the first and second coordination shells for the atom pairs indicated. The distance ranges used were 2-3 and 3-5 Å, for the first and second coordination shells, respectively.

4. CONCLUSION

We have investigated the NMR relaxation mechanism of two Lithium isotopes, ^{7}Li and ^{6}Li, in H_2O and D_2O solvents over a wide range of concentration (0-20) molal to obtain insights into the dynamics of Li-ions, and to determine the breakdown of the relaxation mechanisms, especially at higher concentrations. Our results of T_1 relaxation time and viscosity measurements indicate that the difference between the ^{7}Li relaxation times in D_2O and H_2O is primarily due to the viscosity difference and the presence of ^{7}Li-^{1}H dipolar relaxation in H_2O-based solutions. The quadrupolar moment of ^{6}Li is 50 times weaker than the one of ^{7}Li, which allows separating out the quadrupolar relaxation contribution when comparing T_1 from both isotopes. In addition, molecular dynamics simulations provided

estimates for the electric field gradients and the relevant correlation times from which relaxation was computed. The quadrupolar relaxation contribution was shown to be the most significant relaxation mechanism over most of the concentration range, especially at high concentrations. Combining this quadrupolar contribution with the dipolar contributions obtained from comparing ^{6}Li and ^{7}Li relaxation, showed excellent agreement with the experimentally observed ^{7}Li relaxation rates. The study of these relaxation mechanisms via NMR spectroscopy could be of relevance for investigating the role of lithium-ions in electrochemical processes.

Data availability statement:

The data that support the findings of this study are available from the corresponding author upon reasonable request.

Acknowledgements:

The work was supported by the National Science Foundation under award CBET 1804723.

5. REFERENCES

(1) Balbuena, P. B.; Wang, Y. *Lithium-Ion Batteries: Solid-Electrolyte Interphase*; Imperial College Press, 2004.

(2) Suo, L.; Borodin, O.; Gao, T.; Olguin, M.; Ho, J.; Fan, X.; Luo, C.; Wang, C.; Xu, K. "Water-in-Salt" Electrolyte Enables High-Voltage Aqueous Lithium-Ion Chemistries. *Science* **2015**, *350* (6263), 938–943. https://doi.org/10.1126/science.aab1595.

(3) Kim, H.; Hong, J.; Park, K.-Y.; Kim, H.; Kim, S.-W.; Kang, K. Aqueous Rechargeable Li and Na Ion Batteries. *Chem. Rev.* **2014**, *114* (23), 11788–11827. https://doi.org/10.1021/cr500232y.

(4) Li, W.; Dahn, J. R.; Wainwright, D. S. Rechargeable Lithium Batteries with Aqueous Electrolytes. *Science* **1994**, *264* (5162), 1115–1118. https://doi.org/10.1126/science.264.5162.1115.

(5) Wang, Y.; Yi, J.; Xia, Y. Recent Progress in Aqueous Lithium-Ion Batteries. *Adv. Energy Mater.* **2012**, *2* (7), 830–840. https://doi.org/10.1002/aenm.201200065.

(6) Brown, C. J. The Crystal Structure of Ethylene Carbonate. *Acta Crystallogr.* **1954**, *7* (1), 92–96. https://doi.org/10.1107/S0365110X54000175.

(7) Mason, P. E.; Ansell, S.; Neilson, G. W.; Rempe, S. B. Neutron Scattering Studies of the Hydration Structure of Li+. *J. Phys. Chem. B* **2015**, *119* (5), 2003–2009. https://doi.org/10.1021/jp511508n.

(8) Miller, D. J.; Lisy, J. M. Hydrated Alkali-Metal Cations: Infrared Spectroscopy and Ab Initio Calculations of M+(H2O)X=2−5Ar Cluster Ions for M = Li, Na, K, and Cs. *J. Am. Chem. Soc.* **2008**, *130* (46), 15381–15392. https://doi.org/10.1021/ja803665q.

(9) Morcrette, M.; Chabre, Y.; Vaughan, G.; Amatucci, G.; Leriche, J.-B.; Patoux, S.; Masquelier, C.; Tarascon, J.-M. In Situ X-Ray Diffraction Techniques as a Powerful Tool to Study Battery Electrode Materials. *Electrochimica Acta* **2002**, *47* (19), 3137–3149. https://doi.org/10.1016/S0013-4686(02)00233-5.

(10) Woessner, D. E.; Snowden, B. S.; Ostroff, A. G. Nuclear Spin–Lattice Relaxation in LiCl Solutions. *J. Chem. Phys.* **1968**, *49* (1), 371–375. https://doi.org/10.1063/1.1669832.

(11) Langer, H.; Hertz, H. G. The Structure of the First Hydration Sphere of Ions in Electrolyte Solutions A Nuclear Magnetic Relaxation Study. *Berichte Bunsenges. Für Phys. Chem.* **1977**, *81* (5), 478–490. https://doi.org/10.1002/bbpc.19770810506.

(12) Wehrli, F. W. Temperature-Dependent Spin-Lattice Relaxation of ^{6}Li in Aqueous Lithium Chloride. *J. Magn. Reson.* **1976**, *23* (3), 527–532.

(13) Fabricand, B. P.; Goldberg, S. S. Proton Relaxation Times in 7LiCl and 6LiCl Solutions. *Mol. Phys.* **1967**, *13* (4), 323–330. https://doi.org/10.1080/00268976700101161.

(14) Hertz, H. G.; Tutsch, R.; Versmold, H. Molecular Motion and Structure around the Hydrated Ions Li^{+} and Al^{3+}. *Berichte Bunsenges. Für Phys. Chem.* **1971**, *75* (11), 1177–1191. https://doi.org/10.1002/bbpc.19710751108.

(15) Carof, A.; Salanne, M.; Charpentier, T.; Rotenberg, B. On the Microscopic Fluctuations Driving the NMR Relaxation of Quadrupolar Ions in Water. *J. Chem. Phys.* **2015**, *143* (19), 194504. https://doi.org/10.1063/1.4935496.

(16) Carof, A.; Salanne, M.; Charpentier, T.; Rotenberg, B. Collective Water Dynamics in the First Solvation Shell Drive the NMR Relaxation of Aqueous Quadrupolar Cations. *J. Chem. Phys.* **2016**, *145* (12), 124508. https://doi.org/10.1063/1.4963682.

(17) Carof, A.; Salanne, M.; Charpentier, T.; Rotenberg, B. Accurate Quadrupolar NMR Relaxation Rates of Aqueous Cations from Classical Molecular Dynamics. *J. Phys. Chem. B* **2014**, *118* (46), 13252–13257. https://doi.org/10.1021/jp5105054.

(18) Kowalewski, J.; Maler, L. *Nuclear Spin Relaxation in Liquids: Theory, Experiments, and Applications, Second Edition*; CRC Press, 2017.

(19) Sundholm, D.; Pyykkö, P.; Laaksonen, L.; Sadlej, A. J. Nuclear Quadrupole Moment of Lithium from Combined Fully Numerical and Discrete Basis-Set Calculations on LiH. *Chem. Phys. Lett.* **1984**, *112* (1), 1–9. https://doi.org/10.1016/0009-2614(84)87030-X.

(20) Harris, R. K.; Becker, E. D.; Cabral de Menezes, S. M.; Goodfellow, R.; Granger, P. NMR Nomenclature: Nuclear Spin Properties and Conventions for Chemical Shifts: IUPAC Recommendations 2001. *Solid State Nucl. Magn. Reson.* **2002**, *22* (4), 458–483. https://doi.org/10.1006/snmr.2002.0063.

(21) Badu, S.; Truflandier, L.; Autschbach, J. Quadrupolar NMR Spin Relaxation Calculated Using Ab Initio Molecular Dynamics: Group 1 and Group 17 Ions in Aqueous Solution. *J. Chem. Theory Comput.* **2013**, *9* (9), 4074–4086. https://doi.org/10.1021/ct400419s.

(22) Jerschow, A. From Nuclear Structure to the Quadrupolar NMR Interaction and High-Resolution Spectroscopy. *Prog. Nucl. Magn. Reson. Spectrosc.* **2005**, *46* (1), 63–78. https://doi.org/10.1016/j.pnmrs.2004.12.001.

(23) Abragam, A. *The Principles of Nuclear Magnetism*; Clarendon Press, 1961.

(24) Mao, X.; Guo, J.; Ye, C. Nuclear-Magnetic-Resonance Line-Shape Theory in the Presence of Radiation Damping. *Phys. Rev. B* **1994**, *49* (22), 15702–15711. https://doi.org/10.1103/PhysRevB.49.15702.

(25) Mao, X.; Ye, C. Line Shapes of Strongly Radiation‐damped Nuclear Magnetic Resonance Signals. *J. Chem. Phys.* **1993**, *99* (10), 7455–7462. https://doi.org/10.1063/1.465727.

(26) Wehrli, F. W. Spin-Lattice Relaxation of Some Less Common Weakly Quadrupolar Nuclei. *J. Magn. Reson. 1969* **1978**, *30* (2), 193–209. https://doi.org/10.1016/0022-2364(78)90095-1.